KIAS-P10024

Higgs production in CP-violating supersymmetric cascade decays: probing the 'open hole' at the Large Hadron Collider

Priyotosh Bandyopadhyay[a 1]

Korea Institute for Advanced Study
Hoegiro 87(207-43 Cheongnyangni-dong),
Dongdaemun-gu, Seoul 130-722, Korea

Abstract

A benchmark CP-violating supersymmetric scenario (known as 'CPX-scenario' in the literature) is studied in the context of the Large Hadron Collider (LHC). It is shown that the LHC, with low to moderate accumulated luminosity, will be able to probe the existing 'hole' in the m_{h_1}-$\tan\beta$ plane, which cannot be ruled out by the LEP data. We explore the parameter space with cascade decay of third generation squarks and gluino with CP-violating decay branching fractions. We propose a multi-channel analysis to probe this parameter space some of which are background free at an integrated luminosity of 5-10 fb^{-1}. Specially, multi-lepton final states ($3l$, $4l$ and like sign di-lepton) are almost background free and have 5σ reach for the corresponding signals with very early data of LHC for both 14 TeV and 7 TeV center of mass energy.

[1]priyotosh@kias.re.kr

1 Introduction

One of the main motivations for suggesting supersymmetry (SUSY) is to remove the fine-tuning problem in the Higgs sector of the standard model. The condition of holomorphicity of the superpotential requires two Higgs doublets in the minimal SUSY extension of the standard model (SM). There the Higgs sector has a larger particle content than the SM, and the physical states in this sector comprise two neutral scalars, one pseudoscalar and one charged Higgs boson. Finding the signatures of these scalars is also important along with the search for SUSY at the upcoming Large Hadron Collider (LHC).

Prior to the LHC several experiments failed to discover the Higgs, but yielded some bound on the Higgs mass. The strongest lower bound on the smallest Higgs mass (m_h) from the Large Electron Positron Collider (LEP) is $m_h > 114.4$ GeV [1, 2]. In the MSSM, with all the real and CP-conserving parameters, the lower limit on the lightest Higgs boson is ~ 90 GeV [3] for any $\tan\beta$. However, when the Higgs sector inherits some CP-violating phase through radiative corrections [4, 5], the above limit ceases to be valid. We will be concentrating in this CP-violating scenario.

CP-violation in the Higgs sector is possible in multi-Higgs doublet models, such as a general 2-Higgs Doublet Model (2HDM) or indeed the MSSM. In the latter, it has been shown that, assuming universality of the gaugino masses ($M_i, i = 1, 2, 3$) at some high energy scale, the CP-violating MSSM Higgs sector can be parametrised in terms of two independent phases: that of the Higgsino mass parameter (also called μ term), i.e., Arg(μ), and that of the soft trilinear Supersymmetry (SUSY) breaking parameters, i.e., Arg(A_f), with $f = t, b$. The experimental upper bounds on the Electric Dipole Moments (EDMs) of electrons and neutrons [6, 7] as well as of mercury atoms [8] constraints on these phases.

It is well-known by now that the lower bound on the mass of the lightest Higgs boson of the CP-conserving MSSM (from LEP [2]) can be drastically reduced or may even entirely vanish if non-zero CP-violating phases are allowed [9, 10]. This can happen through radiative corrections to the Higgs potential, whereby the above mentioned phases of the Higgsino mass parameter μ and the trilinear soft SUSY breaking parameter A enter into the picture. As a result of the CP-violating phase, the neutral spinless states are no more of definite parity, and their couplings to gauge bosons as well as fermions are thus modified, depending on the magnitude of the phases. Thus there are three neutral states h_i (i=1,2,3); the collider search limits for all of them are modified since the squared amplitudes for production via WW, ZZ and $q\bar{q}$ couplings for all of them now consist of more than one term. Due to this mixing through the loop effects, the lightest Higgs boson is almost CP-odd with highly suppressed coupling to ZZ pair. Thus results in reduced production rates and consequent weakening of mass limits at collider experiments.

In the context of a benchmark CP-violating scenario (often called the CPX scenario in the literature [10]), it has been found that m_{h_1} as low as 50 GeV or even smaller, cannot be ruled out by the final LEP data for low and moderate values of $\tan\beta$,[2]. In other words, a 'hole' is found to exist in the m_{h_1}-$\tan\beta$ parameter space covered by the LEP searches, the underlying reason being the reduction in the coupling ZZh_1 due to the CP-violating phase(s), as mentioned above. Moreover, complementary channels such as $e^+e^- \to h_1h_2$, suffer from coupling as well as phase-space suppression within this 'hole', thus making it inaccessible to LEP searches. The existence of this hole has been confirmed by the analysis of the LEP data by different experimental groups [2], although its span varies.

The next natural step is to assess the prospect of closing the hole at Tevatron Run II or the LHC. The existing analysis on this [11], however, focuses on the discovery channels based on the conventional Higgs production and decay mechanisms employed in the context of the SM. It has been noted that although the hadron colliders can probe most of the parameter space of the CPX scenario and can indeed go beyond some regions of the parameter space scanned by the LEP searches, the lightest Higgs boson within the aforementioned hole may still escape detection. This is because not only the ZZh_1 but also the WWh_1 and $t\bar{t}h_1$ couplings tend to be very small within this hole. On the other hand, the relatively heavy neutral Higgs bosons $h_{2,3}$ couple to W, Z and t favourably, but they can decay in non-standard channels, thus requiring a modification in search strategies. The other work [13] which has looked into possible signals of the CPX scenario at the LHC is also restricted to the production of h_i (i=1,2,3) bosons in SM-like channels. However, they looked into more decay channels of the h_i bosons thus produced. Until now it has been concluded that parts of the holes in the M_H^+-$\tan\beta$ or the m_{h_1}-$\tan\beta$ parameter space can be plugged, although considerable portions of the hole, especially for low $\tan\beta$, may escape detection at the LHC even after accumulating 300 fb^{-1} of integrated luminosity.

Thus it is important to look for other production channels for the scalars in the CPX region, especially by making use of the couplings of h_1 with the sparticles. In this context we explore the cascade decay of third generation scalar quarks, mainly $\tilde{t}_1\tilde{t}_1^*$ and $\tilde{b}_1\tilde{b}_1^*$. This could be discovery channels, in cases where the t-$\bar{t}$-h_1 and W-W-h_1, Z-Z-h_1 couplings are highly suppressed.

Previously, measurement of CP-asymmetries and the various decays probing this CP-violating sector have been studied extensively [[12]-[25]]. The Higgs production under the CP-conserving supersymmetric cascade has been analysed in Refs. [26, 27, 28, 29, 30]. It has been noted that in a general CP-violating MSSM, the cross section of $\tilde{t}_1\tilde{t}_1^*h_1$ production could be dramatically larger than that obtained by switching off the

[2]where h_1 is the lightest neutral Higgs, and $\tan\beta$ is the ratio of the vacuum expectation values of the two Higgs doublets

CP-violating phases [31]. Since the trilinear SUSY breaking parameter A_t is necessarily large in the CPX scenario, $\tilde{t}_1$ tends to be relatively light and may be produced at the LHC with large cross section. As a bonus, both h_2 and h_3 also couple favourably to the $t\bar{t}$ pair and can add modestly to the signal although by themselves they fail to produce a statistically significant signal. In Ref. [32] we investigated the implications of these couplings at the LHC, by concentrating on a specific signal arising from the associated production of the neutral Higgs bosons with a top-pair or a pair of lighter stop squarks.

This paper is organised as follows. In Section 2 we discuss the basic inputs of the CPX scenario, the resulting mass spectrum and other features they lead to. All of our subsequent numerical analysis would be in this framework where we also use the alternative expression CPV-SUSY to mean the CPX-scenario. In section 3 we define the proposed parton level signal. In section 4 we do the collider simulation and devise the event selection criteria to reduce the SM backgrounds and present the final numerical results in section 5. We summarise and conclude in section 6.

2 The CPX Model: values of various parameters

As indicated in the introduction, we adopt the so called CPX scenario in which the LEP analyses have been performed. It has been observed [4, 5] that the CP-violating quantum effects on the Higgs potential is proportional to $Im(\mu A_t)/M^2_{SUSY}$, where A_t is the trilinear soft SUSY breaking parameter occurring in the top squark mass matrix, and M_{SUSY} is the characteristic SUSY breaking scale, which is of the order of the third generation squark masses. With this in mind, a benchmark scenario known as CPX was proposed and its consequences were studied [33, 34, 35, 36, 37, 38, 39, 40, 41, 42]. In this scenario, the effects of CP-violation are maximized. The corresponding inputs that we adopt here are compatible with the "hole" left out in the analysis.

$$
\begin{aligned}
& m_{\tilde{t}} = m_{\tilde{b}} = m_{\tilde{\tau}} = M_{SUSY} = 500 \text{ GeV}, \qquad \mu = 4M_{SUSY} = 2 \text{ TeV} \\
& |A_t| = |A_b| = 2M_{SUSY} = 1 \text{ TeV}, \quad arg(A_{t,b}) = 90^\circ \\
& |m_{\tilde{g}}| = 1 \text{ TeV}, \quad arg(m_{\tilde{g}}) = 90^\circ \\
& M_2 = 2M_1 = 200 \text{ GeV}, \quad \tan\beta = 5 - 10
\end{aligned}
$$

The only departure from reference [11] lies in a small tweaking in the mass ratio of the $U(1)$ and $SU(2)$ gaugino masses M_1 and M_2, aimed at ensuring gaugino mass unification at high scale. It has been checked that this difference does not affect the Higgs production or the decay rates. The presence of a relatively large A_t ensures that one of the top squarks will be relatively light. The value of the top quark mass has

m_{h_1}	m_{h_2}	m_{h_3}	$m_{\tilde{t}_1}$	$m_{\tilde{t}_2}$	$m_{\tilde{b}_1}$	$m_{\tilde{b}_2}$	$m_{\chi_1^0}$	$m_{\chi_2^0}$	$m_{\chi_1^\pm}$
39.8	104.7	137.1	317.6	668.2	475.9	526.6	99.6	198.4	198.4

Table 1: Physical masses (in GeV) of neutral Higgs bosons, squarks and lighter gauginos in the CPX scenario with $\tan\beta$=5 and $m_{H^\pm}$=130 GeV with the threshold corrections.

$\sigma_{\tilde{t}_1\tilde{t}_1^*}$	$\sigma_{\tilde{b}_1\tilde{b}_1^*}$	$\sigma_{\tilde{t}_2\tilde{t}_2^*}$	$\sigma_{\tilde{b}_2\tilde{b}_2^*}$	$\sigma_{\tilde{t}_1\tilde{t}_2}$	$\sigma_{\tilde{b}_1\tilde{b}_2}$	$\sigma_{\tilde{t}_i\tilde{b}_j}$	$\sigma_{\tilde{g}\tilde{g}}$
2861	323.3	4	178.5	8	0.6	7	135

Table 2: Production cross sections (in fb) at lowest-order computed with `CalcHEP` interfaced with CPsuperH for different signal processes at the LHC in the CPX scenario and for the spectrum of Table 1. `CTEQ6L` parton distribution functions are used and the renormalization/factorization scale is set to $\sqrt{\hat{s}}$.

been taken to be 175 GeV[3].

It is to be noted that the first two generation sfermion masses must be kept sufficiently heavy so that the stringent experimental bound (for example, the electric dipole moment of the neutron) is satisfied. Here we have not considered possible ways of bypassing such bounds, and set the masses of the first two sfermion families at 10 TeV. Thus our analysis is based on the mass spectrum showed in Table 1 with $\tan\beta$=5 and $m_{H^\pm}$=130 GeV with the threshold corrections and considered as benchmark point 1(BP1).The cross sections for different supersymmetric production processes are computed with `CalcHEP` [43] (interfaced with the program `CPSuperH`[44, 45]). For the benchmark point 1(BP1) the cross-section for different supersymmetric processes are listed in the Table 2. The cross-sections of the associated Higgs production within the model have been given in Table 3.

As we will be focusing on the cascade decay of the third generation strongly interacting supersymmetric particles (squarks) and gluino we should also see how the branching fraction changes down the cascade compared to CP-conserving SUSY scenario. For the bench mark point we list the the branching fractions for $\tilde{t}_1$, $\tilde{b}_1$, $\tilde{g}$ and the Higgses in the Tables 4, 5, 6, 7 respectively. Here the charged Higgs which is produced in the cascade decay goes through an unconventional decay mode $H^\pm \to h_1 W^\pm$ due to

[3]The frequent shift in the central value of m_t, coming from Tevatron measurements, causes the size of the hole to change, although its location remains the same. However, there is little point in worrying about this uncertainty, since the very quantum corrections which are at the root of all CP-violating effects in the Higgs sector are prone to similar, if not greater, theoretical uncertainties

$\sigma_{t\bar{t}h_1}$	$\sigma_{t\bar{t}h_2}$	$\sigma_{t\bar{t}h_3}$
8	190	132

Table 3: Production cross sections (in fb) at lowest-order computed with `CalcHEP` interfaced with CPsuperH for different signal processes at the LHC in the CPX scenario and for the spectrum of Table 1. `CTEQ6L` parton distribution functions are used and the renormalization/factorization scale is set to $\sqrt{\hat{s}}$.

$\mathrm{Br}(\tilde{t}_1 \to b\chi_1^+)$	$\mathrm{Br}(\tilde{t}_1 \to t\chi_1^0)$
0.81	0.19

Table 4: Branching fractions for lighter top squark in the CPX scenario.

the low m_{h_1} in CPX scenario. Mainly due to this all the signal topologies get changed that is from the CP-conserving SUSY scenario.

3 Collider signatures

In this section we will discuss the cascade decays of third generation squarks under the CPX scenario. First consider the $\tilde{t}_1\tilde{t}_1^*$. When both the $\tilde{t_1}$ decays via $\tilde{t_1} \to t\chi_1^0$ then we have the following final states at the end.

$$\begin{aligned} pp \to \tilde{t_1}\tilde{t_1}^* &\to t\bar{t}\chi_1^0\chi_1^0 \to b\bar{b}H^+H^-\chi_1^0\chi_1^0 \\ &\to b\bar{b}W^+W^-h_1h_1\chi_1^0\chi_1^0 \\ &\to 6b + 4(non-b)jet + \not{p}_T \\ &\to 6b + l + 2(non-b)jet + \not{p}_T \\ &\to 6b + OSD + \not{p}_T \end{aligned}$$

But $\mathrm{Br}(t \to bH^+) \simeq 0.011$ due to which the effective branching fraction, i.e. $\mathrm{Br}(\tilde{t}_1\tilde{t}_1^* \to b\bar{b}H^+H^-\chi_1^0\chi_1^0) \simeq 5 \times 10^{-8}$. Thus above channels which could have been interesting and could have added to the signal cross-section those coming from $\tilde{b_1}\tilde{b_1}^*$ no longer do

$\mathrm{Br}(\tilde{b}_1 \to \tilde{t}_1H^-)$	$\mathrm{Br}(\tilde{b}_1 \to \tilde{t}_1W^-)$	$\mathrm{Br}(\tilde{b}_1 \to t\chi_1^-)$	$\mathrm{Br}(\tilde{b}_1 \to b\chi_2^0)$	$\mathrm{Br}(\tilde{b}_1 \to b\chi_1^0)$
0.77	0.12	0.05	0.04	0.01

Table 5: Branching fractions for lighter bottom squark in the CPX scenario.

$\mathrm{Br}(\tilde{g} \to b\tilde{b}_1)$	$\mathrm{Br}(\tilde{g} \to b\tilde{b}_2)$	$\mathrm{Br}(\tilde{g} \to t\tilde{t}_1)$	$\mathrm{Br}(\tilde{g} \to t\tilde{t}_2)$
0.28	0.24	0.32	0.16

Table 6: Branching fractions for gluino in the CPX scenario.

$\mathrm{Br}(H^{\pm} \to h_1 W^{\pm})$	$\mathrm{Br}(h_1 \to b\bar{b})$	$\mathrm{Br}(h_2 \to h_1 h_1)$	$\mathrm{Br}(h_3 \to h_1 h_1)$
0.84	0.92	0.85	0.82

Table 7: Branching fractions for Higgs bosons in the CPX scenario.

so. There are other modes coming from $\tilde{t}_1\tilde{t}_1^*$ which could be interesting. For example, the case where one of the $\tilde{t}_1$ decays via $\tilde{t}_1 \to b\chi_1^+$ and this gives rise to the following signal signal topologies.

$$\tilde{t_1}\tilde{t_1}^* \to t\bar{b}\chi_1^0\chi_1^- \to b\bar{b}H^+W^-\chi_1^0\chi_1^0 \to b\bar{b}h_1W^+W^-\chi_1^0\chi_1^0$$
$$\to 4b + 4(non-b)jet + \not{p}_T$$
$$\to 4b + 1(non-b)jet + 1\ell + \not{p}_T$$
$$\to 4b + OSD + \not{p}_T$$

Now we consider the other pair production of the third generation scalar quark, the sbottom pair production. As given in Table 2 s the production cross section is about 323 fb. Due to large branching fraction in $\tilde{b_1} \to \tilde{t_1}H^-$ (Table 5), in the main decay mode, both of the sbottoms decay in this channel. Then due to large branching fraction of $H^{\pm} \to h_1W^{\pm}$ (Table 7) we end up with $4W + 2h_1 + 2b + \not{p}_T$. Depending on the decay mode of w we can have the following final states.

$$pp \to \tilde{b_1}\tilde{b_1}^* \to \tilde{t_1}\tilde{t_1}^*H^+H^- \to b\bar{b}W^+W^-W^+W^-h_1h_1 + \not{p}_T$$
$$\to 6b + LSD + 4(non-b)jet + \not{p}_T$$
$$\to 6b + 3\ell + 2(non-b)jet + \not{p}_T$$
$$\to 6b + 4\ell + \not{p}_T$$

The contribution of gluino pair production comes from the gluino decays to these stops and sbottoms (Table 2 and Table 6). As for this CPX parameter space, mass of the gluino is taken to be heavier than the third generation scalar quarks, so this cross-section just adds to the signal cross-section (either stop or sbottom). Below we list the effective cross-section of different channels coming from third generation scalar squark decays (stop and sbottom pairs).

Number of channels	Channels	Effective cross-sec (in fb)
1	$6b + LSD + 4(non-b)jet + \not{p}_T$	11.49
1	$6b + OSD + 4(non-b)jet + \not{p}_T$	22.98
2	$6b + 3\ell + 2(non-b)jet + \not{p}_T$	17.24
3	$6b + 4\ell + \not{p}_T$	8.62
4	$4b + 4(non-b)jet + \not{p}_T$	0.38
5	$4b + 1(non-b)jet + 1\ell + \not{p}_T$	0.18
6	$4b + OSD + \not{p}_T$	0.09

Table 8: Production cross sections (in fb) at lowest-order computed with `CalcHEP` interfaced with CPsuperH for different signal processes at the LHC in the CPX scenario and for the spectrum of Table 1. `CTEQ6L` parton distribution functions are used and the renormalization/factorization scale is set to $\sqrt{\hat{s}}$.

The channels coming from $\tilde{b_1}\tilde{b_1}^*$ are absolutely background free at the partonic level. So these could be golden channels to probe CPX. It is the $\tilde{b_1}\tilde{b_1}^*$ which could produce multiple b-s in the final state. It is very clear from Table 8 that the multiple b processes, like the $4b$ processes coming from $\tilde{t_1}\tilde{t_1}^*$ have very low cross-section. But because of ISR/FSR and jet smearing, the parton level predictions could change. For that purpose we go through a PYTHIA [46] simulation to analyse the signals and backgrounds in the next section.

4 Collider study

In this study, `CalcHEP` (interfaced to the program `CPSuperH`) has also been used for generating parton-level events for the relevant processes. The standard `CalcHEP-PYTHIA` interface [49], which uses the SLHA interface [50] was then used to pass the `CalcHEP`-generated events to `PYTHIA` [46]. Further, all relevant decay-information is generated with `CalcHEP` and is passed to `PYTHIA` through the same interface. All these are required since there is no public implementation of CPV-MSSM in `PYTHIA`. Subsequent decays of the produced particles, hadronization and the collider analyses are done with `PYTHIA (version 6.4.22)`.

We used `CTEQ6L` parton distribution function (PDF) [47, 48]. In `CalcHEP` we opted for the lowest order α_s evaluation, which is appropriate for a lowest order PDF like `CTEQ6L`. The renormalization/factorization scale in `CalcHEP` is set at $\sqrt{\hat{s}}$. This choice of scale results in a somewhat conservative estimate for the event rates.

In the CPX scenario, although h_1 decays dominantly into $b\bar{b}$, our simulation reveals

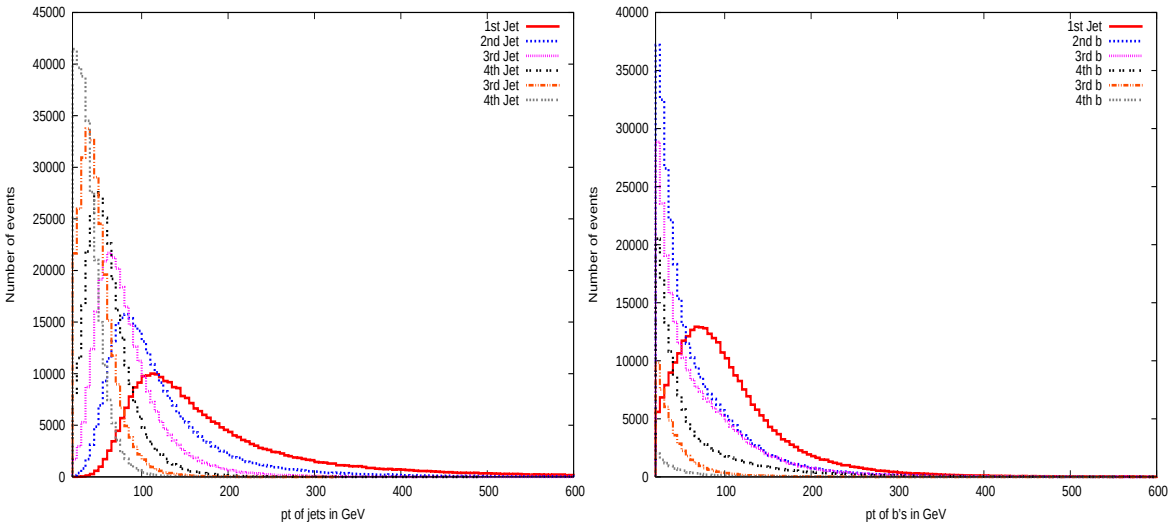

Figure 1: Ordered p_T^{jet} (left) and parton level b p_T distributions in CPV-SUSY scenario for $\tilde{b}_1\tilde{b}_1^*$

that in a fairly large fraction of events both the b-quarks do not lead to sufficiently hard jets with reasonable b-tagging efficiency. This is because of the lightness of h_1 in this scenario. To illustrate this, we present in Figure 1 the ordered p_T distributions for the four parton-level b-quarks in the signal from $\tilde{b}_1\tilde{b}_1^*$. It is clear from this figure that the b-quark with the lowest p_T in a given event is often below 40 GeV or thereabout, which could have ensured a moderate tagging efficiency ($\geq 50\%$).

For hadronic level simulation we have used `PYCELL`, the toy calorimeter simulation provided in `PYTHIA`, with the following criteria:

- the calorimeter coverage is $|\eta| < 4.5$ and the segmentation is given by $\Delta\eta \times \Delta\phi = 0.09 \times 0.09$ which resembles a generic LHC detector
- a cone algorithm with $\Delta R = \sqrt{\Delta\eta^2 + \Delta\phi^2} = 0.5$ has been used for jet finding
- $p_{T,min}^{jet} = 20$ GeV and jets are ordered in p_T
- leptons ($\ell = \mathrm{e},\ \mu$) are selected with $p_T \geq 20$ GeV and $|\eta| \leq 2.5$
- no jet should match with a hard lepton in the event

From the Figure 1 it is very clear that the parton level distributions are reflected in the PYCELL level jets. From the p_Ts of the jets and b's it is clear that there are two b's or jets having p_T greater than 100 GeV, which are coming from the $\tilde{t}_1$'s. On the other hand the b's coming from the light Higgs h are of low p_Ts.

From Figure 2 we can see that the jet multiplicity for the $\tilde{t}_1\tilde{t}_1^*$ is higher than of $t\bar{t}$ which is true for $\tilde{b}_1\tilde{b}_1^*$ and $\tilde{g}\tilde{g}$ as well. So higher jet multiplicity cut will reduce the $t\bar{t}$ as well as the other Standard Model (SM) backgrounds. Figure 3 and 4 show the lepton

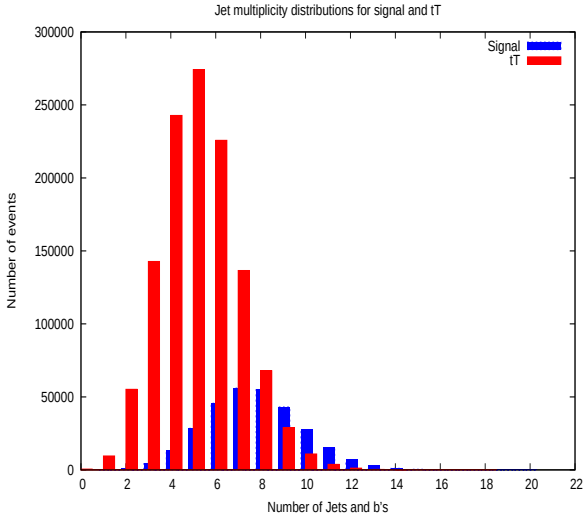

Figure 2: Jet multiplicity distributions in CPV-SUSY scenario for $\tilde{t}_1\tilde{t}_1^*$ and $t\bar{t}$

p_T and multiplicity distributions. These figures suggest that we can have some hard leptons in the final states that will also kill the SM backgrounds; specially with higher multiplicity.

We also compare the missing p_T distributions of $\tilde{b}_1\tilde{b}_1^*$ and $t\bar{t}$ in Figure 5 which suggests that $\not{p}_T \geq 100$ GeV will kill the sufficient amount of $t\bar{t}$ events.

The possible backgrounds are very less because of higher jet multiplicity and higher number of b-jets, leptons and missing energy for the signal topologies. But still for the signal topologies with lower number of b-jets and leptons can have some Standard model backgrounds. These are $t\bar{t}$, $t\bar{t}Z$, $t\bar{t}t\bar{t}$, $t\bar{t}b\bar{b}$. In particular ISR/FSR can increase the jet multiplicity of these backgrounds and these should be considered. Among these $t\bar{t}t\bar{t}$ cross-sec is very low (of the order few fb), [4]. We calculated other potential backgrounds by CalcHEP-PYTHIA [49] and AlPGEN-PYTHIA interfacing [51].

5 Results

Below we have analysed few signal topologies for the case of bench mark point 1(BP1). Table 9 presents the contributions to the signals for different supersymmetric cascade decays. In all we have taken nine different signal topologies. Out of these, the first six are of higher jet-multiplicities and the remaining topologies are of relatively low jet multiplicities ($n_{jet} \geq 4$). Table 9 gives the number for an integrated luminosity of 10 fb^{-1}. From Table 9 it is clear that for higher jet-multiplicity $\tilde{t}_1\tilde{t}_1^*$ does not have much contribution as explained in Section 3. It contributes mostly for the low jet multiplicity

[4]Checked with Alpgen [51]

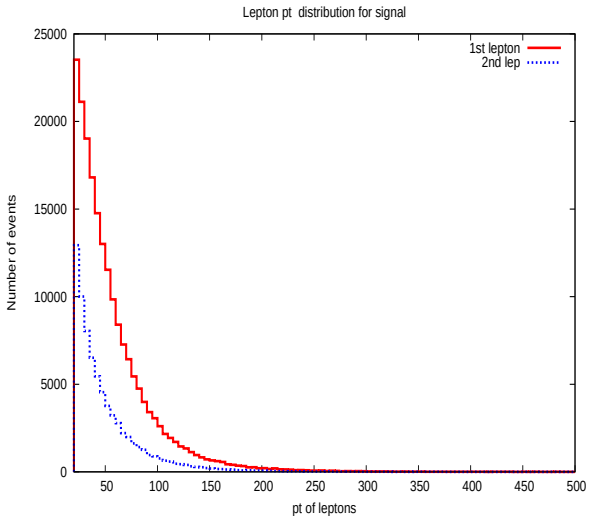

Figure 3: Lepton p_T distributions in CPV-SUSY scenario for $\tilde{t}_1\tilde{t}_1^*$

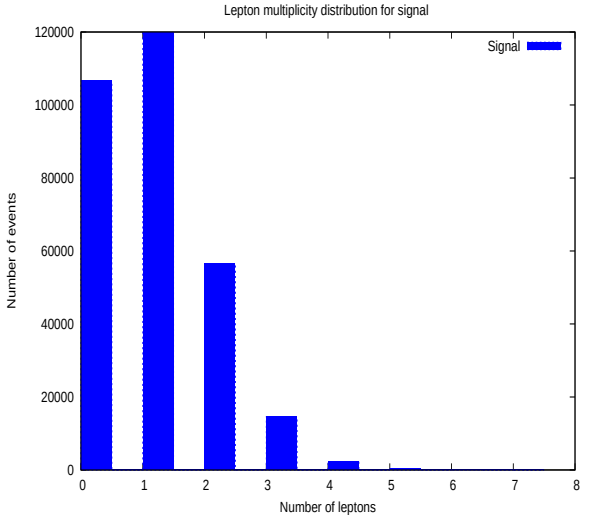

Figure 4: Lepton multiplicity distributions in CPV-SUSY scenario for $\tilde{t}_1\tilde{t}_1^*$

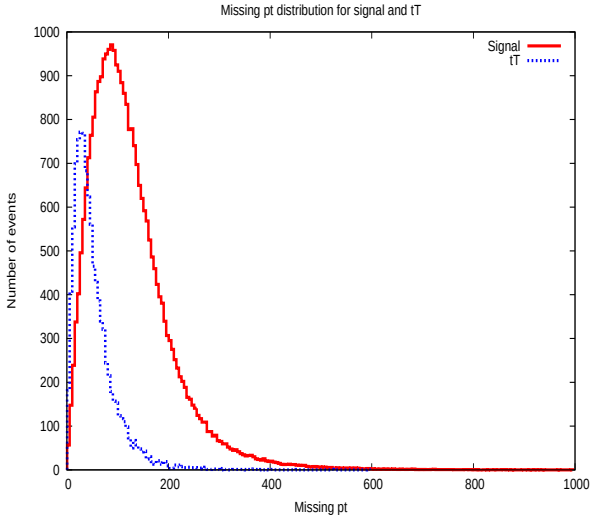

Figure 5: Missing p_T distributions in CPV-SUSY scenario for $\tilde{b}_1\tilde{b}_1^*$ and $t\bar{t}$

signals. For the higher jet multiplicity the maximum contribution comes from $\tilde{g}\tilde{g}$.

The corresponding main SM backgrounds are listed in Table 10 for an integrated luminosity of 10 fb^{-1}. Comparing Table 9 and Table 10 we can get a significance $\geq 10\sigma$ for almost all the signal topologies except signal topology 7; which is of 4.81σ. Now as we have discussed in Section 3. Out of all the jets there are two $b-jets$ which are of high p_T coming from the $\tilde{t}_1$ decay which are not there in case of the SM backgrounds. So we demand the first and the second highest jets to have p_T greater than 100 GeV. The event rates with this cuts are given in the brackets of Table 9 and Table 10. Implementation of these cuts increases the signal significance by 10-20%.

Next we extend this analysis to the other points of the 'LEP-hole' and show the viability of these signals in other regions of the CPX hole. It has already been noted in the literature that the size and the exact location of the hole in the parameter space depend on the method of calculating the loop corrections [45, 52, 53]. However, the calculations agree qualitatively and confirm the presence of the hole. To be specific we have chosen points from the hole as presented by [9].

In Table 11 we varied $\tan\beta$ and $m_{H^\pm}$ keeping the other parameters fixed. These correspond to three more different regions of the LEP hole and are termed as benchmark points 2 -4 (BP2 - BP4), all within the hole. We computed the sensitivity for all of these points; both signals and backgrounds. The results are summarised in Tables 12, 13, 14, 15, 16, 17. These results suggest that the LEP-hole can be probed with an integrated luminosity of 5-10 fb^{-1} as like in the benchmark point 1. However, the multilepton channels, e.g., $3l$, $4l$ and like sign di-lepton being almost background free, have 5σ reach with very early data of the LHC. So with the early data of LHC every corner of the 'hole' is expected to be probed via these cascade decays. For $\sqrt{S} = 7$

No.	Signal topology	$\tilde{b}_1\tilde{b}_1^*$	$\tilde{t}_1\tilde{t}_1^*$	$\tilde{g}\tilde{g}$
1	$n_{jet} \geq 8(b-\text{jet} \geq 3) + l \geq 2 + \not{p}_T \geq 100$	10(5.6)	0.4(0.2)	53(52.8)
2	$n_{jet} \geq 8(b-\text{jet} \geq 3) + l \geq 2(\text{OSD} \geq 1) + \not{p}_{\text{T}} \geq 100$	7(3.9)	0.4(0.2)	37(36.7)
3	$n_{jet} \geq 8(b-\text{jet} \geq 3) + l \geq 2(\text{SSD} \geq 1) + \not{p}_{\text{T}} \geq 100$	4(2.2)	0(0)	23(22.1)
4	$n_{jet} \geq 8(b-\text{jet} \geq 2) + l \geq 3 + \not{p}_T \geq 100$	2(1.1)	0(0)	8(8)
5	$n_{jet} \geq 8(b-\text{jet} \geq 2) + l \geq 4 + \not{p}_T \geq 100$	0(0)	0(0)	1(0.8)
6	$n_{jet} \geq 8(b-\text{jet} \geq 4) + l \geq 2 + \not{p}_T \geq 100$	3(1.5)	0(0)	34(33.2)
7	$n_{jet} \geq 4(b-\text{jet} \geq 3) + l \geq 1 + \not{p}_T \geq 100$	116(63.6)	45(26.2)	283(279.3)
8	$n_{jet} \geq 4(b-\text{jet} \geq 3) + l \geq 2(\text{OSD} \geq 1) + \not{p}_{\text{T}} \geq 100$	21(9.7)	4(1.9)	54(52.9)
9	$n_{jet} \geq 8(b-\text{jet} \geq 3) + \not{p}_T \geq 100$	149(96.3)	46(34.2)	499(498)

Table 9: Event rates for the CPX point(BP1) of an integrated luminosity of 10 fb^{-1}

No.	Signal topology	$t\bar{t}$	$t\bar{t}Z$	$t\bar{t}b\bar{b}$
1	$n_{jet} \geq 8(b-\text{jet} \geq 3) + l \geq 2 + \not{p}_T \geq 100$	19(13)	0.33(0.27)	6.1(4.6)
2	$n_{jet} \geq 8(b-\text{jet} \geq 3) + l \geq 2(\text{OSD} \geq 1) + \not{p}_{\text{T}} \geq 100$	17(12)	0.29(.23)	6.1(4.6)
3	$n_{jet} \geq 8(b-\text{jet} \geq 3) + l \geq 2(\text{SSD} \geq 1) + \not{p}_{\text{T}} \geq 100$	3(1)	0.05(0.05)	0(0)
4	$n_{jet} \geq 8(b-\text{jet} \geq 2) + l \geq 3 + \not{p}_T \geq 100$	0(0)	0.27(0.19)	0(0)
5	$n_{jet} \geq 8(b-\text{jet} \geq 2) + l \geq 4 + \not{p}_T \geq 100$	0(0)	0.0(0.0)	0(0)
6	$n_{jet} \geq 8(b-\text{jet} \geq 4) + l \geq 2 + \not{p}_T \geq 100$	5(5)	0.08(0.05)	2.6(2.4)
7	$n_{jet} \geq 4(b-\text{jet} \geq 3) + l \geq 1 + \not{p}_T \geq 100$	1890(953)	22.6(13.21)	297.1 (170.4)
8	$n_{jet} \geq 4(b-\text{jet} \geq 3) + l \geq 2(\text{OSD} \geq 1) + \not{p}_{\text{T}} \geq 100$	226(101)	2.7(1.4)	34.2(16.6)
9	$n_{jet} \geq 8(b-\text{jet} \geq 3) + \not{p}_T \geq 100$	1109(784)	13.4(10.5)	252.3(185.6)

Table 10: Event rates for the CPX point(BP1) of an integrated luminosity of 10 fb^{-1}

Parameters	BP2	BP3	BP4
$\tan\beta$	4.0	4.0	7.0
$m_{H^\pm}$	140	135	125
m_{h_1} (GeV)	49.45	33.8	40.8

Table 11: Benchmark points within the LEP-hole in m_{h_1}-$\tan\beta$ plane.

No.	Signal topology	$\tilde{b}_1\tilde{b}_1^*$	$\tilde{t}_1\tilde{t}_1^*$	$\tilde{g}\tilde{g}$
1	$n_{jet} \geq 8(b-\text{jet} \geq 3) + l \geq 2 + \not{p}_T \geq 100$	14.1(7.8)	0.19(0.10)	58.4(56.5)
2	$n_{jet} \geq 8(b-\text{jet} \geq 3) + l \geq 2(\text{OSD} \geq 1) + \not{p}_{\text{T}} \geq 100$	10.1(5.6)	0.19(0.10)	40.0(38.7)
3	$n_{jet} \geq 8(b-\text{jet} \geq 3) + l \geq 2(\text{SSD} \geq 1) + \not{p}_{\text{T}} \geq 100$	5.2(2.8)	0(0)	26.1(25.2)
4	$n_{jet} \geq 8(b-\text{jet} \geq 2) + l \geq 3 + \not{p}_T \geq 100$	1.8(1.0)	0(0)	9.5(9.1)
5	$n_{jet} \geq 8(b-\text{jet} \geq 2) + l \geq 4 + \not{p}_T \geq 100$	0(0)	0(0)	0.6(0.6)
6	$n_{jet} \geq 8(b-\text{jet} \geq 4) + l \geq 2 + \not{p}_T \geq 100$	4.6(2.5)	0.1(0)	36.3(38.7)
7	$n_{jet} \geq 4(b-\text{jet} \geq 3) + l \geq 1 + \not{p}_T \geq 100$	146.3(78.6)	44.8(23.4)	296.0(289.4)
8	$n_{jet} \geq 4(b-\text{jet} \geq 3) + l \geq 2(\text{OSD} \geq 1) + \not{p}_{\text{T}} \geq 100$	26.9(12.6)	3.3(1.4)	56.5(54.5)
9	$n_{jet} \geq 8(b-\text{jet} \geq 3) + \not{p}_T \geq 100$	196.6(123.7)	48.5(34.0)	516.6(510.7)

Table 12: Event rates for the CPX point(BP2) of an integrated luminosity of 10 fb^{-1}

TeV, the production cross-sections are given in Table 18. From Table 18 it is clear that the cross-sections for $\sqrt{S} = 7$ TeV are reduced by the factor of ~ 10, whereas the main background $t\bar{t}$ is reduced by a factor of ~ 6. These make the reach possible for higher luminosity, though $3l$, $4l$ and like sign di-lepton channels, which are almost background free can be still observed with the early data of the LHC (a few fb^{-1}).

On top of this multi-channel analysis we try get the invariant mass peak for the light Higgs boson. In that case it would of great help in probing the CP-violating light Higgs boson as well as killing all the backgrounds which include the model background as well. Among the all different signal topologies we have taken $n - jet \geq 6\,(3\,b - jets) + 4\,\text{leptons} + \not{p}_{\text{T}} \geq 150\,\text{GeV} + \text{m}_{\text{eff}} \geq 100\,\text{GeV}$ which has the best reach. Here we define m_{eff} as scalar sum of missing-p_T, jet-p_Ts and lepton-p_Ts. Figure 6 shows the invariant mass of two b-jets in this final state topology for benchmark point 1. The figure clearly shows a peak around light Higgs boson mass which is around 40 GeV. On top of this at integrated luminosity of 10 fb^{-1} no $t\bar{t}$ event passes the above signal criteria to contribute in the invariant mass distribution as backgrounds. The mass peak also very useful to kill all the other model backgrounds. Thus, reconstruction of the light Higgs boson mass peak could be an indicator of the CP-violating Higgs discovery.

The effective masses and couplings at one loop depend on the soft masses, i.e., M_{SUSY}, that contribute in the loop. Thus, the $Z - Z - h_1$ coupling as well the shape of the 'LEP hole' change with the variation of M_{SUSY}. In principle there could be some regions where m_{h_1} is still light (≤ 60 GeV) but ruled out by LEP because of the $Z-Z-h_1$ coupling is large. From [54] we see that when M_{SUSY} increases the 'LEP hole' almost vanishes, as the mixing term in the Higgs mass matrix, i.e., $M_{\text{SP}} \simeq \frac{\mu^2 A}{M_{\text{SUSY}}}$ goes to zero. In page 62 and Figure 28 of [54] describes two different scenarios corresponding

No.	Signal topology	$t\bar{t}$	$t\bar{t}Z$	$t\bar{t}b\bar{b}$
1	$n_{jet} \geq 8(b-\text{jet} \geq 3) + l \geq 2 + \not{p}_T \geq 100$	19(12)	0.33(0.25)	3.4(1.9)
2	$n_{jet} \geq 8(b-\text{jet} \geq 3) + l \geq 2(\text{OSD} \geq 1) + \not{p}_{\text{T}} \geq 100$	17(10)	0.30(.22)	3.4(1.9)
3	$n_{jet} \geq 8(b-\text{jet} \geq 3) + l \geq 2(\text{SSD} \geq 1) + \not{p}_{\text{T}} \geq 100$	3(3)	0.07(0.05)	0(0)
4	$n_{jet} \geq 8(b-\text{jet} \geq 2) + l \geq 3 + \not{p}_T \geq 100$	0(0)	0.17(0.10)	0(0)
5	$n_{jet} \geq 8(b-\text{jet} \geq 2) + l \geq 4 + \not{p}_T \geq 100$	0(0)	0.0(0.0)	0(0)
6	$n_{jet} \geq 8(b-\text{jet} \geq 4) + l \geq 2 + \not{p}_T \geq 100$	2(1)	0.12(0.08)	1.9(0.9)
7	$n_{jet} \geq 4(b-\text{jet} \geq 3) + l \geq 1 + \not{p}_T \geq 100$	1950(952)	23.0(13.4)	314.2(172.6)
8	$n_{jet} \geq 4(b-\text{jet} \geq 3) + l \geq 2(\text{OSD} \geq 1) + \not{p}_{\text{T}} \geq 100$	226(98)	2.6(1.4)	33.5(15.4)
9	$n_{jet} \geq 8(b-\text{jet} \geq 3) + \not{p}_T \geq 100$	1056(733)	14.69(11.14)	265.9(187.2)

Table 13: Event rates for the CPX point(BP2) of an integrated luminosity of 10 fb^{-1}

No.	Signal topology	$\tilde{b}_1\tilde{b}_1^*$	$\tilde{t}_1\tilde{t}_1^*$	$\tilde{g}\tilde{g}$
1	$n_{jet} \geq 8(b-\text{jet} \geq 3) + l \geq 2 + \not{p}_T \geq 100$	13.2(7.4)	0.57(0.57)	54.52(53.00)
2	$n_{jet} \geq 8(b-\text{jet} \geq 3) + l \geq 2(\text{OSD} \geq 1) + \not{p}_{\text{T}} \geq 100$	9.1(5.1)	0.57(0.57)	37.09(36.04)
3	$n_{jet} \geq 8(b-\text{jet} \geq 3) + l \geq 2(\text{SSD} \geq 1) + \not{p}_{\text{T}} \geq 100$	5.2(2.8)	0(0)	23.18(22.48)
4	$n_{jet} \geq 8(b-\text{jet} \geq 2) + l \geq 3 + \not{p}_T \geq 100$	1.7(0.9)	0(0)	7.33(6.93)
5	$n_{jet} \geq 8(b-\text{jet} \geq 2) + l \geq 4 + \not{p}_T \geq 100$	0.1(0)	0(0)	0.82(0.65)
6	$n_{jet} \geq 8(b-\text{jet} \geq 4) + l \geq 2 + \not{p}_T \geq 100$	4.3(2.2)	0.28(0.28)	34.39(33.39)
7	$n_{jet} \geq 4(b-\text{jet} \geq 3) + l \geq 1 + \not{p}_T \geq 100$	134.1(72.2)	43.87(20.78)	287.66(282.32)
8	$n_{jet} \geq 4(b-\text{jet} \geq 3) + l \geq 2(\text{OSD} \geq 1) + \not{p}_{\text{T}} \geq 100$	24.4(11.4)	4.76(2.38)	53.41(51.82)
9	$n_{jet} \geq 8(b-\text{jet} \geq 3) + \not{p}_T \geq 100$	179.9(114.5)	50.45(33.66)	494.04(488.58)

Table 14: Event rates for the CPX point(BP3) of an integrated luminosity of 10 fb^{-1}

No.	Signal topology	$t\bar{t}$	$t\bar{t}Z$	$t\bar{t}b\bar{b}$
1	$n_{jet} \geq 8(b-\text{jet} \geq 3) + l \geq 2 + \not{p}_T \geq 100$	9(5)	0.32(0.21)	6.8(3.9)
2	$n_{jet} \geq 8(b-\text{jet} \geq 3) + l \geq 2(\text{OSD} \geq 1) + \not{p}_{\text{T}} \geq 100$	9(5)	0.29(.18)	6.5(3.7)
3	$n_{jet} \geq 8(b-\text{jet} \geq 3) + l \geq 2(\text{SSD} \geq 1) + \not{p}_{\text{T}} \geq 100$	3(3)	0.07(0.03)	0.2(0.2)
4	$n_{jet} \geq 8(b-\text{jet} \geq 2) + l \geq 3 + \not{p}_T \geq 100$	0(0)	0.27(0.20)	0(0)
5	$n_{jet} \geq 8(b-\text{jet} \geq 2) + l \geq 4 + \not{p}_T \geq 100$	0(0)	0.0(0.0)	0(0)
6	$n_{jet} \geq 8(b-\text{jet} \geq 4) + l \geq 2 + \not{p}_T \geq 100$	1(0)	0.10(0.05)	2.9(1.7)
7	$n_{jet} \geq 4(b-\text{jet} \geq 3) + l \geq 1 + \not{p}_T \geq 100$	1250(491)	22.05(12.43)	313.8(174.5)
8	$n_{jet} \geq 4(b-\text{jet} \geq 3) + l \geq 2(\text{OSD} \geq 1) + \not{p}_{\text{T}} \geq 100$	130(41)	2.90(1.32)	38.5(17.1)
9	$n_{jet} \geq 8(b-\text{jet} \geq 3) + \not{p}_T \geq 100$	473(266)	13.99(10.44)	254.9(178.2)

Table 15: Event rates for the CPX point(BP3) of an integrated luminosity of 10 fb^{-1}

No.	Signal topology	$\tilde{b}_1\tilde{b}_1^*$	$\tilde{t}_1\tilde{t}_1^*$	$\tilde{g}\tilde{g}$
1	$n_{jet} \geq 8(b-\text{jet} \geq 3) + l \geq 2 + \not{p}_T \geq 100$	3.39(2.09)	0.19(0.09)	50.53(49.24)
2	$n_{jet} \geq 8(b-\text{jet} \geq 3) + l \geq 2(\text{OSD} \geq 1) + \not{p}_{\text{T}} \geq 100$	2.36(1.44)	0.09(0.00)	33.86(33.04)
3	$n_{jet} \geq 8(b-\text{jet} \geq 3) + l \geq 2(\text{SSD} \geq 1) + \not{p}_{\text{T}} \geq 100$	1.28(0.80)	0(0)	22.18(21.48)
4	$n_{jet} \geq 8(b-\text{jet} \geq 2) + l \geq 3 + \not{p}_T \geq 100$	0.74(0.51)	0(0)	7.28(6.98)
5	$n_{jet} \geq 8(b-\text{jet} \geq 2) + l \geq 4 + \not{p}_T \geq 100$	0.03(0.03)	0(0)	0.47(0.47)
6	$n_{jet} \geq 8(b-\text{jet} \geq 4) + l \geq 2 + \not{p}_T \geq 100$	0.63(0.37)	0(0)	29.40(28.76)
7	$n_{jet} \geq 4(b-\text{jet} \geq 3) + l \geq 1 + \not{p}_T \geq 100$	66.47(38.48)	41.47(21.74)	314.14(307.86)
8	$n_{jet} \geq 4(b-\text{jet} \geq 3) + l \geq 2(\text{OSD} \geq 1) + \not{p}_{\text{T}} \geq 100$	10.18(5.18)	4.01(2.00)	59.22(57.16)
9	$n_{jet} \geq 8(b-\text{jet} \geq 3) + \not{p}_T \geq 100$	77.26(52.73)	47.11(34.01)	521.51(515.17)

Table 16: Event rates for the CPX point(BP4) of an integrated luminosity of 10 fb^{-1}

No.	Signal topology	$t\bar{t}$	$t\bar{t}Z$	$t\bar{t}b\bar{b}$
1	$n_{jet} \geq 8(b-\text{jet} \geq 3) + l \geq 2 + \not{p}_T \geq 100$	9(4)	0.29(0.23)	3.7(3.1)
2	$n_{jet} \geq 8(b-\text{jet} \geq 3) + l \geq 2(\text{OSD} \geq 1) + \not{p}_T \geq 100$	9(4)	0.25(.21)	2.9(2.4)
3	$n_{jet} \geq 8(b-\text{jet} \geq 3) + l \geq 2(\text{SSD} \geq 1) + \not{p}_T \geq 100$	3(3)	0.07(0.05)	0.7(0.7)
4	$n_{jet} \geq 8(b-\text{jet} \geq 2) + l \geq 3 + \not{p}_T \geq 100$	0(0)	0.18(0.10)	0(0)
5	$n_{jet} \geq 8(b-\text{jet} \geq 2) + l \geq 4 + \not{p}_T \geq 100$	0(0)	0.0(0.0)	0(0)
6	$n_{jet} \geq 8(b-\text{jet} \geq 4) + l \geq 2 + \not{p}_T \geq 100$	1(1)	0.09(0.07)	0.9(0.7)
7	$n_{jet} \geq 4(b-\text{jet} \geq 3) + l \geq 1 + \not{p}_T \geq 100$	1049(420)	21.43(12.58)	310.6(168.2)
8	$n_{jet} \geq 4(b-\text{jet} \geq 3) + l \geq 2(\text{OSD} \geq 1) + \not{p}_T \geq 100$	105(30)	2.42(1.30)	38.6(16.1)
9	$n_{jet} \geq 8(b-\text{jet} \geq 3) + \not{p}_T \geq 100$	412(244)	13.70(10.15)	258.8(184.1)

Table 17: Event rates for the CPX point(BP4) of an integrated luminosity of 10 fb^{-1}

$\sigma_{\tilde{t}_1\tilde{t}_1^*}$	$\sigma_{\tilde{b}_1\tilde{b}_1^*}$	$\sigma_{\tilde{b}_2\tilde{b}_2^*}$	$\sigma_{\tilde{g}\tilde{g}}$
288.7	21.9	10.6	0.7

Table 18: Production cross sections (in fb) at lowest-order computed with `CalcHEP` interfaced with CPsuperH for different processes at the LHC in the CPX scenario and for the spectrum of Table 1 for $\sqrt{s} = 7$ TeV. `CTEQ6L` parton distribution functions are used and the renormalization/factorization scale is set to $\sqrt{\hat{s}}$.

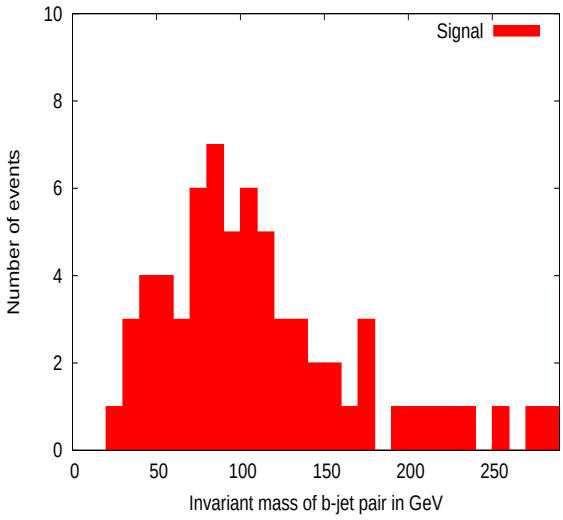

Figure 6: Invariant mass of b-jet pair for benchmark point 1

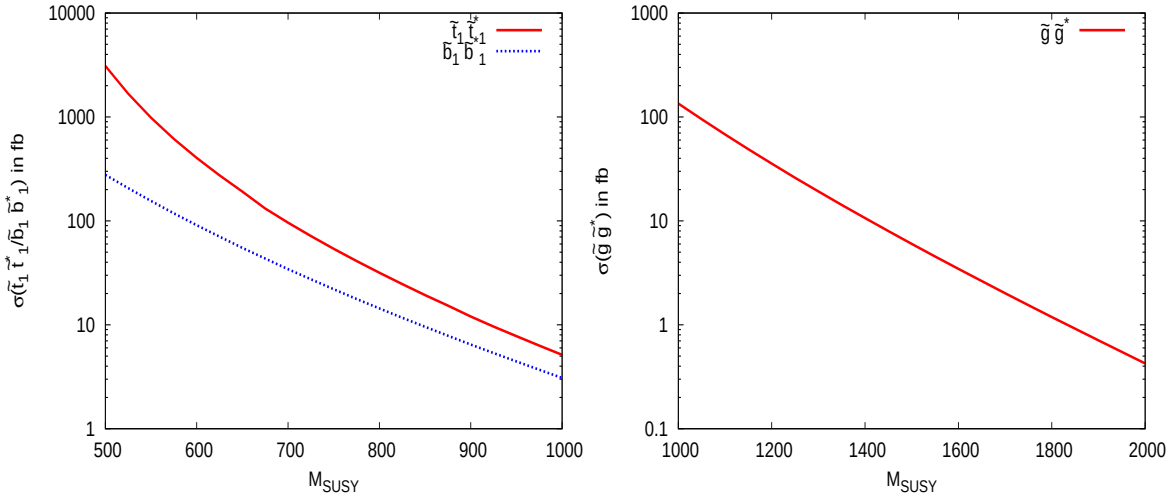

Figure 7: Cross-sec variation of with $M_{\rm SUSY}$ for $\tilde{t}_1\tilde{t}_1^*$, $\tilde{b}_1\tilde{b}^*$ (left) and $\tilde{g}\tilde{g}$ (right)

to $M_{\rm SUSY} = 1$ TeV as given below.

1. **CPX1.0:**

   $\mu = 4M_{\rm SUSY}$, $\quad |A| = 2M_{\rm SUSY}$, $\quad |M_3| = 2M_{\rm SUSY}$.

   For this case with $M_{\rm SUSY} = 1$TeV the hole is still there near $m_{h_1} = 30 - 60$ GeV.

2. **CPX0.5:**

   Where $M_{\rm SUSY} = 1$ TeV for third generation squark masses but all the other parameters kept in the as normal CPX, i.e. corresponding to $M_{\rm SUSY} = 500$ GeV case as before. For this case the 'hole' is shifted to $m_{h_1} \geq 75$ GeV.

Figure 7 describe the variation of the production cross-section of the $\tilde{t}_1\tilde{t}_1^*$, $\tilde{b}_1\tilde{b}_1^*$ and $\tilde{g}\tilde{g}$ with $M_{\rm SUSY}$ respectively. From the figures it is very clear that the cross-sections drops down very fast as $M_{\rm SUSY}$ increases. Thus the cross-sections for the **CPX0.5**, **CPX1.0** decrease, resulting lowering of events for the final states. In Table 19 and Table 20 present the number of events for the **CPX0.5**, **CPX1.0** for the integrated luminosity of 10 fb^{-1}. The numbers suggest that for the **CPX0.5** we still get 5σ signal significance over the SM backgrounds for most of the signal topologies. This is because the gluino contribution is still large, as in **CPX0.5** the $|m_{\tilde{g}}| = 1$TeV; which is same as the normal CPX scenario. Where as for **CPX1.0** none of the final states get 5σ significance for 10 fb^{-1} of integrated luminosity. The signal 8, which is having best significance over the background, will require 128 fb^{-1} of integrated luminosity for the 5σ significance over the SM backgrounds.

In our choice of parameter points, we have $M_1 = 100$ GeV, $M_2 = 200$ GeV and $M_{\rm SUSY} = 500$ GeV for all the first four benchmark points. In those cases stop has two decay modes; $\tilde{t}_1 \to t\chi_1^0$ and $\tilde{t}_1 \to b\chi_1^+$. But as we increase $M_{\rm SUSY}$ to higher values other

No.	Signal topology	$\tilde{b}_1\tilde{b}_1^*$	$\tilde{t}_1\tilde{t}_1^*$	$\tilde{g}\tilde{g}$
1	$n_{jet} \geq 8(b-\text{jet} \geq 3) + l \geq 2 + \not{p}_T \geq 100$	0.18(0.18)	0.06(0.05)	34.11(32.75)
2	$n_{jet} \geq 8(b-\text{jet} \geq 3) + l \geq 2(\text{OSD} \geq 1) + \not{p}_\text{T} \geq 100$	0.15(0.14)	0.06(0.05)	23.18(22.51)
3	$n_{jet} \geq 8(b-\text{jet} \geq 3) + l \geq 2(\text{SSD} \geq 1) + \not{p}_\text{T} \geq 100$	0.06(0.06)	0.01(0.01)	13.89(13.07)
4	$n_{jet} \geq 8(b-\text{jet} \geq 2) + l \geq 3 + \not{p}_T \geq 100$	0.04(0.04)	0(0)	4.18(3.91)
5	$n_{jet} \geq 8(b-\text{jet} \geq 2) + l \geq 4 + \not{p}_T \geq 100$	0.01(0.01)	0(0)	0.40(0.40)
6	$n_{jet} \geq 8(b-\text{jet} \geq 4) + l \geq 2 + \not{p}_T \geq 100$	0.06(0.06)	0.04(0.03)	20.09(19.01)
7	$n_{jet} \geq 4(b-\text{jet} \geq 3) + l \geq 1 + \not{p}_T \geq 100$	2.43(2.29)	3.24(2.96)	238.88(226.20)
8	$n_{jet} \geq 4(b-\text{jet} \geq 3) + l \geq 2(\text{OSD} \geq 1) + \not{p}_\text{T} \geq 100$	0.35(0.31)	0.36(0.31)	40.85(37.34)
9	$n_{jet} \geq 8(b-\text{jet} \geq 3) + \not{p}_T \geq 100$	3.33(3.25)	4.16(4.08)	396.06(384.37)

Table 19: Event rates for the CPX0.5 of an integrated luminosity of 10 fb^{-1}

No.	Signal topology	$\tilde{b}_1\tilde{b}_1^*$	$\tilde{t}_1\tilde{t}_1^*$	$\tilde{g}\tilde{g}$
1	$n_{jet} \geq 8(b-\text{jet} \geq 3) + l \geq 2 + \not{p}_T \geq 100$	0.16(0.15)	0.12(0.11)	0.25(0.25)
2	$n_{jet} \geq 8(b-\text{jet} \geq 3) + l \geq 2(\text{OSD} \geq 1) + \not{p}_\text{T} \geq 100$	0.11(0.11)	0.09(0.09)	0.17(0.17)
3	$n_{jet} \geq 8(b-\text{jet} \geq 3) + l \geq 2(\text{SSD} \geq 1) + \not{p}_\text{T} \geq 100$	0.06(0.05)	0.03(0.02)	0.12(0.12)
4	$n_{jet} \geq 8(b-\text{jet} \geq 2) + l \geq 3 + \not{p}_T \geq 100$	0.03(0.03)	0(0)	0.04(0.04)
5	$n_{jet} \geq 8(b-\text{jet} \geq 2) + l \geq 4 + \not{p}_T \geq 100$	0.01(0.01)	0(0)	0.01(0.01)
6	$n_{jet} \geq 8(b-\text{jet} \geq 4) + l \geq 2 + \not{p}_T \geq 100$	0.05(0.05)	0.07(0.06)	0.17(0.17)
7	$n_{jet} \geq 4(b-\text{jet} \geq 3) + l \geq 1 + \not{p}_T \geq 100$	2.54(2.40)	6.32(5.64)	1.33(1.33)
8	$n_{jet} \geq 4(b-\text{jet} \geq 3) + l \geq 2(\text{OSD} \geq 1) + \not{p}_\text{T} \geq 100$	0.43(0.38)	0.56(0.43)	0.23(0.23)
9	$n_{jet} \geq 8(b-\text{jet} \geq 3) + \not{p}_T \geq 100$	3.68(3.58)	9.48(9.12)	2.35(2.35)

Table 20: Event rates for the CPX1.0 of an integrated luminosity of 10 fb^{-1}

decay modes of stop could also be open. In principle stop can decay to $t\chi_2^0$ (in the case of **CPX0.5**, **CPX1.0**) as shown below. The χ_2^0 thus produced, can have two-body or three body decays depending on the parameter points which will enrich the final state at the end

$$\begin{aligned}\tilde{t}_1 \to t\chi_2^0 &\to tll\chi_1^0 \\ &\to tZ/h\chi_1^0\end{aligned}$$

. Along with the above mentioned decay modes, we could have the following decay and also to higher neutralino modes.

$$\begin{aligned}\tilde{t}_1 \to b\chi_2^+ &\to bH^+\chi_1^0 \\ &\to bW^+\chi_1^0\end{aligned}$$

But, in the CPX scenario, $\mu = 4M_{\rm SUSY}$, which makes the higher charginos and neutralinos as Higgsino type, thus much heavier than the corresponding stop mass eigen states. This results in making these decay modes kinematically disallowed.

6 Summary and Conclusions

We have explored supersymmetric cascade decays in the context of CP-violating MSSM and important for the CPX scenario. This cascade decay analysis can also probe the 'LEP-hole' in the CPX scenario with the early data from LHC. These final states in the CPX scenario are a consequence of low mass of the lightest Higgs boson (as light as 30 GeV). The invariant mass distribution of these b-jets also peaks around the lightest neutral Higgs boson. This kills all the model and other backgrounds. Moreover, multi-lepton final states ($3l$, $4l$ and like sign di-lepton) are easy to detect as they are almost background free; thus have 5σ reach for the corresponding signals with very early data of LHC for both 14 TeV and 7 TeV center of mass energy. We have also studied the range of sensitivity for $M_{\rm SUSY} = 1$ TeV for **CPX0.5** and **CPX1.0** in this context. We found that though 5σ reach is possible for **CPX0.5** with 10 fb^{-1} of data, for **CPX1.0** one needs to go beyond 100 fb^{-1} data. Also heavier stop in these cases can lead to richer final states through its decay to Higgs(es) or leptons. Finally the supersymmetric cascades under CP-violating scenario are very different from the CP-conserving case because of the possible non-trivial decay modes in the former case.

Acknowledgments: I would like to thank Prof. Michael Peskin for pointing out to this problem of third generation supersymmetric cascade decays in the CP-violating scenario. I would also like to thank Prof. Amitava Datta, Prof. Manuel Drees, Prof. Biswarup Mukhopadhyaya and Dr. AseshKrishna Datta for the useful discussions. I

also thank Ms. Nabanita Bhattacharyya for the discussion regarding b-tagging. Computational work for this study was partially carried out in the cluster computing facility at Harish-Chandra Research Institute (HRI) (http://cluster.mri.ernet.in).

References

[1] R. Barate *et al.* [LEP Working Group for Higgs boson searches], Phys. Lett. B **565**, 61 (2003) [arXiv:hep-ex/0306033];
see also $http://lephiggs.web.cern.ch/LEPHIGGS/www/Welcome.html$

[2] S. Schael *et al.* [ALEPH Collaboration], Eur. Phys. J. C **47**, 547 (2006) [arXiv:hep-ex/0602042];
see also $http://lephiggs.web.cern.ch/LEPHIGGS/www/Welcome.html$

[3] See: LEP SUSY Working Group, `http://lepsusy.web.cern.ch/lepsusy`, and LEP Higgs Working Group,`LHWG-Note 2004-01`.

[4] A. Pilaftsis, Phys. Rev. D **58**, 096010 (1998) [arXiv:hep-ph/9803297].

[5] A. Pilaftsis, Phys. Lett. B **435**, 88 (1998) [arXiv:hep-ph/9805373].

[6] P. Nath, Phys. Rev. Lett. **66**, 2565 (1991); Y. Kizukuri and N. Oshimo, Phys. Rev. D **46**, 3025 (1992); T. Ibrahim and P. Nath Phys. Lett. B **418**, 98 (1998); Phys. Rev. D **57**, 478 (1998); *ibid* D **58**, 019901(E) (1998); *ibid* D **60**, 079903 (1999); *ibid* D **60**, 119901 (1999); M. Brhlik, G.J. Good and G.L. Kane, Phys. Rev. D **59**, 115004 (1999); A. Bartl, T. Gajdosik, W. Porod, P. Stockinger and H. Stremnitzer, Phys. Rev. D **60**, 073003 (1999); D. Chang, W.-Y. Keung and A. Pilaftsis, Phys. Rev. Lett. **82**, 900 (1999); S. Pokorski, J. Rosiek and C.A. Savoy, Nucl. Phys. B **570**, 81 (2000); E. Accomando, R. Arnowitt and B. Dutta, Phys. Rev. D **61**, 115003 (2000); S. Abel, S. Khalil and O. Lebedev, Nucl. Phys. B **606**, 151 (2001); U. Chattopadhyay, T. Ibrahim and D.P. Roy, Phys. Rev. D **64**, 013004 (2001); D.A. Demir, M. Pospelov and A. Ritz, hep-ph/0208257. J. R. Ellis, J. S. Lee and A. Pilaftsis, JHEP **0810**, 049 (2008) [arXiv:0808.1819 [hep-ph]].

[7] A. Pilaftsis, Nucl. Phys. B **644**, 263 (2002).

[8] T. Falk, K.A. Olive, M. Pospelov and R. Roiban, Nucl. Phys. B **60**, 3 (1999).

[9] P. Bechtle [LEP Collaboration], PoS **HEP2005**, 325 (2006) [arXiv:hep-ex/0602046].

[10] M. S. Carena, J. R. Ellis, A. Pilaftsis and C. E. M. Wagner, Phys. Lett. B **495**, 155 (2000) [arXiv:hep-ph/0009212].

[11] M. S. Carena, J. R. Ellis, S. Mrenna, A. Pilaftsis and C. E. M. Wagner, Nucl. Phys. B **659**, 145 (2003) [arXiv:hep-ph/0211467].

[12] D. K. Ghosh, R. M. Godbole, D. P. Roy, Phys. Lett. **B628** (2005) 131-140. [hep-ph/0412193]. D. K. Ghosh, S. Moretti, Eur. Phys. J. **C42** (2005) 341-347. [hep-ph/0412365].

[13] E. Accomando *et al.*, [arXiv:hep-ph/0608079].

[14] F. F. Deppisch and O. Kittel, JHEP **1006** (2010) 067 [arXiv:1003.5186 [hep-ph]].

[15] P. Draper, T. Liu and C. E. M. Wagner, Phys. Rev. D **81** (2010) 015014 [arXiv:0911.0034 [hep-ph]].

[16] A. C. Fowler and G. Weiglein, JHEP **1001** (2010) 108 [arXiv:0909.5165 [hep-ph]].

[17] A. De Roeck *et al.*, Eur. Phys. J. C **66** (2010) 525 [arXiv:0909.3240 [hep-ph]].

[18] S. W. Ham, S. A. Shim and S. K. Oh, Phys. Rev. D **80** (2009) 055009 [arXiv:0907.3300 [hep-ph]].

[19] F. Deppisch and O. Kittel, JHEP **0909** (2009) 110 [Erratum-ibid. **1003** (2010) 091] [arXiv:0905.3088 [hep-ph]].

[20] G. Weiglein, Nucl. Phys. Proc. Suppl. **183** (2008) 149.

[21] J. S. Lee, AIP Conf. Proc. **1078** (2009) 36 [arXiv:0808.2014 [hep-ph]].

[22] A. Djouadi and R. M. Godbole, arXiv:0901.2030 [hep-ph].

[23] O. Kittel and F. von der Pahlen, JHEP **0808** (2008) 030 [arXiv:0806.4534 [hep-ph]].

[24] K. E. Williams and G. Weiglein, Phys. Lett. B **660** (2008) 217 [arXiv:0710.5320 [hep-ph]].

[25] S. P. Das, M. Drees,
[arXiv:1010.3701 [hep-ph]]. S. P. Das, M. Drees,
[arXiv:1010.2129 [hep-ph]].

[26] A. Datta, A. Djouadi, M. Guchait and Y. Mambrini, Phys. Rev. D **65** (2002) 015007 [arXiv:hep-ph/0107271].

[27] A. Datta, A. Djouadi, M. Guchait and F. Moortgat, Nucl. Phys. B **681** (2004) 31 [arXiv:hep-ph/0303095].

[28] P. Bandyopadhyay, A. Datta and B. Mukhopadhyaya, Phys. Lett. B **670** (2008) 5 [arXiv:0806.2367 [hep-ph]].

[29] P. Bandyopadhyay, JHEP **0907** (2009) 102 [arXiv:0811.2537 [hep-ph]].

[30] G. D. Kribs, A. Martin, T. S. Roy and M. Spannowsky, Phys. Rev. D **81**, 111501 (2010) [arXiv:0912.4731 [hep-ph]]. G. D. Kribs, A. Martin, T. S. Roy and M. Spannowsky, Phys. Rev. D **82**, 095012 (2010) [arXiv:1006.1656 [hep-ph]].

[31] Z. Li, C. S. Li and Q. Li, Phys. Rev. D **73**, 077701 (2006) [arXiv:hep-ph/0601148].

[32] P. Bandyopadhyay, A. Datta, A. Datta and B. Mukhopadhyaya, Phys. Rev. D **78** (2008) 015017 [arXiv:0710.3016 [hep-ph]].

[33] A. Pilaftsis and C. E. M. Wagner, Nucl. Phys. B **553**, 3 (1999) [arXiv:hep-ph/9902371].

[34] D. A. Demir, Phys. Rev. D **60**, 055006 (1999) [arXiv:hep-ph/9901389].

[35] S. Y. Choi, M. Drees and J. S. Lee, Phys. Lett. B **481**, 57 (2000) [arXiv:hep-ph/0002287].

[36] G. L. Kane and L. T. Wang, Phys. Lett. B **488**, 383 (2000) [arXiv:hep-ph/0003198].

[37] S. Y. Choi, K. Hagiwara and J. S. Lee, Phys. Rev. D **64**, 032004 (2001) [arXiv:hep-ph/0103294].

[38] S. Y. Choi, K. Hagiwara and J. S. Lee, Phys. Lett. B **529**, 212 (2002) [arXiv:hep-ph/0110138].

[39] S. Heinemeyer, Eur. Phys. J. C **22**, 521 (2001) [arXiv:hep-ph/0108059].

[40] T. Ibrahim and P. Nath, Phys. Rev. D **66**, 015005 (2002) [arXiv:hep-ph/0204092].

[41] S. W. Ham, S. K. Oh, E. J. Yoo, C. M. Kim and D. Son, Phys. Rev. D **68**, 055003 (2003) [arXiv:hep-ph/0205244].

[42] P. Bandyopadhyay and K. Huitu, arXiv:1106.5108 [hep-ph].

[43] A. Pukhov, "CalcHEP 3.2: MSSM, structure functions, event generation, batchs, and generation of matrix elements for other packages", [arXiv:hep-ph/0412191].

[44] J. R. Ellis, J. S. Lee and A. Pilaftsis, Mod. Phys. Lett. A **21**, 1405 (2006) [arXiv:hep-ph/0605288]. J. S. Lee, M. Carena, J. Ellis, A. Pilaftsis and C. E. M. Wagner, Comput. Phys. Commun. **180**, 312 (2009) [arXiv:0712.2360 [hep-ph]].

[45] J. S. Lee, A. Pilaftsis, M. S. Carena, S. Y. Choi, M. Drees, J. R. Ellis and C. E. M. Wagner, Comput. Phys. Commun. **156**, 283 (2004) [arXiv:hep-ph/0307377].

[46] T. Sjostrand, L. Lonnblad and S. Mrenna, [arXiv:hep-ph/0108264].

[47] H. L. Lai *et al.* [CTEQ Collaboration], Eur. Phys. J. C **12**, 375 (2000) [arXiv:hep-ph/9903282].

[48] J. Pumplin, D. R. Stump, J. Huston, H. L. Lai, P. Nadolsky and W. K. Tung, JHEP **0207**, 012 (2002) [arXiv:hep-ph/0201195].

[49] See "http://hep.pa.msu.edu/people/belyaev/public/calchep/index.html"

[50] P. Skands *et al.*, JHEP **0407**, 036 (2004) [arXiv:hep-ph/0311123];
see also $http://home.fnal.gov/skands/slha/$

[51] M. L. Mangano, M. Moretti, F. Piccinini, R. Pittau and A. D. Polosa, JHEP **0307** (2003) 001 [arXiv:hep-ph/0206293].

[52] M. Frank, T. Hahn, S. Heinemeyer, W. Hollik, H. Rzehak and G. Weiglein, JHEP **0702**, 047 (2007) [arXiv:hep-ph/0611326].

[53] T. Hahn, S. Heinemeyer, W. Hollik, H. Rzehak, G. Weiglein and K. Williams, [arXiv:hep-ph/0611373].

[54] G. Abbiendi *et al.* [OPAL Collaboration], Eur. Phys. J. C **37** (2004) 49 [arXiv:hep-ex/0406057].